Simulation of Flow Around Bluff Bodies at High Reynolds Numbers

Guilherme Vaz de Almeida Fontes Neves
guilherme.fontes.neves@tecnico.ulisboa.pt

Instituto Superior Técnico, Universidade de Lisboa, Portugal

January 2021

Abstract

Motivated by a complex off-shore aquaculture structure, this work focuses on statistically unsteady flow around bluff bodies of polygonal cross-section. The RANS equations are used for modeling and closed with turbulence models. Two preliminary studies were performed, the first concluded that unstructured grids were able to accurately perform the simulations around bluff bodies. The second preliminary showed a significant improvement in numerical robustness of the simulations with the use of wall functions. The 3D study of flow around the aquaculture structure at $Re = 10^8$ used unstructured grids with wall functions. Estimations of the average forces and moments acting on the structure were presented, as well as the frequency content.

Keywords: Bluff Bodies, Octagonal Cross-Section, Unstructured Grids, Wall Functions, High Reynolds Number.

1. Introduction

The main objective of this work is to study the forces and moments acting on an aquaculture structure so that an accurate structural analysis can be done in subsequent studies. To achieve this there are two challenges that must be tackled:

- **Complexity of the geometry**: the floating ring is an octagon with sharp obtuse angles ($> \pi$) and other complex geometric details;
- **Reynolds number**: The Reynolds number of the flow is $Re =\approx 10^8$. This is a very high Reynolds number, which presents a computational challenge.

Two preliminary 2D studies were made to tackle these challenges and achieve the best computational set-up for the simulations of flow around the aquaculture structure:

- Preliminary Study 1: The use of **unstructured grids** would simplify the discretization of the domain. This study aimed to verify the quality and numerical robustness of the unstructured grids produced by HEXPRESS^{TM}. The work done in [6] was used as reference.
- Preliminary Study 2: The use of **wall functions** can help lower computation time. This study aims to evaluate the ability to use wall functions in the simulations with flow around bluff bodies at very high Reynolds numbers as well as evaluate the numerical convergence properties of the simulation [5].

2. Background

Bluff bodies in turbulent flow have been the topic of research for many years, with the circular cylinder as the prime subject of the investigation.

However, the study of flow behind infinitely long bluff bodies with a cross section with more than four sides ($N > 4$) has not received the same level of attention. Khaledi and Andersson [6] studied the flow around a finite hexagonal cylinder with 3D geometry using DNS at three different Reynolds numbers ($Re = 100, Re = 500, Re = 1000$) for two orientations of the cylinder: face oriented and corner oriented. They concluded that for wake dynamics, it is irrelevant if the front stagnation point is at a face or a corner but rather "if the width of the projected cylinder is determined by sharp corners or flow-parallel faces". They also speculated that the wake behind a octagonal cylinder would have a behaviour similar to the one after a square cylinder.

Xu et al [18] tested cylinders with $N = 2-8, N = 12, N = 16$ as well as a circular cylinder ($N = \infty$) based on fluid force, hot-wire, Particle Image Velocimetry (PIV) and flow visualisation measurements for a Reynolds number of $10^4 \sim 10^5$. The dependence of C_D and St on the number of faces was studied.

3. Problem Formulation

This section describes the mathematical and geometrical formulation of the investigation.

3.1. RANS Formulation

It is useful to perform a Reynolds decomposition, which will deal with the intrinsically unsteady features of turbulence.

The research that this work focuses on is unsteady in nature, so the Reynolds decomposition for unsteady flows to the Navier-Stokes equation (mass and momentum balance) will be applied, obtaining the, so-called Unsteady Reynolds-Averaged Navier-Stokes Equations (U-RANS).

After performing a Reynolds decomposition and a Reynolds (ensemble) Average, one obtains the needed equations:

$$\frac{\partial(\rho\overline{u_i})}{\partial x_i} = 0 \tag{1}$$

$$\frac{\partial(\rho\overline{u_i})}{\partial t} + \frac{\partial}{\partial x_j}\left(\rho\overline{u_i}\,\overline{u_j} + \rho\overline{u_i'u_j'}\right) = -\frac{\partial\overline{p}}{\partial x_i} + \frac{\partial\overline{\tau_{ij}}}{\partial x_j} \tag{2}$$

where Cartesian coordinates and Tensor notation where used.

The presence of the Reynolds stresses, indicates that the equations are not closed. Turbulence Models are used to close the equations by approximating values for these terms. The $k-\omega SST(2003)$ model [11, 15] and the $KSKL$ model [13, 12] are two such models and will be used in this research.

3.2. Turbulence Models

3.2.1. $k-\omega$ SST (2003) Model

The $k-\omega$ Shear Stress Transport (SST) model was developed by Menter in 1994 [11].

In 2003 Menter published slight variations to his own model [15], the most important being the definition of the eddy viscosity. These changes are then the $k-\omega$ SST (2003) model, which is the model that will be be used throughout this work.

3.2.2. KSKL Model

The KSKL model was derived by Menter et al. based on the k-kL model by Rotta [13, 12].

3.3. Computational Domain

The two preliminary studies and the final 3D study had different objectives and were performed at different Reynolds numbers, so naturally each computational domain is different.

3.3.1. Preliminary Study 1

The domain used for this study tried to recreate the domain used in [6], which was $20d$ long, $16d$ wide and $6d$ high (x, y, z), with the axis of the cylinder centered at ($x = 5.5d$, $y = 8.0d$), where d is the circumscribed diameter of the hexagon. A domain with similar dimensions was created, however the simulations here performed were 2D in nature and as such the length of the cylinder in the z-direction is considered to be infinite. Additionally simulations were also performed on the flow around a circular cylinder and an octagonal cylinder with both orientations (corner-facing and face-facing).

3.3.2. Preliminary Study 2

This study aimed to check the impact of using wall functions on the computation of a flow at a Reynolds number of 10^8. A domain based on previous investigations [1], was designed. The domain was $118d$ long and $102d$ wide, with the center of the cylinder placed in the width-wise centerline of the domain, $51d$, and lengthwise $40d$ away from the inlet. The cylinders studied had circular, octagonal and hexadecagonal cross-sectional shapes.

3.3.3. 3D Study

The final part of this work concerns itself with the flow around the complete aquaculture structure at a Reynolds number of $Re = 10^8$. Some simplifications were made in order to guarantee the feasibility of the simulations:

- The net was considered to be non-permeable and non-deformable, in effect acting as a wall.
- Waves were not considered for the simulations as the Froude Number is very low, $Fr = \frac{U}{\sqrt{gL}} \approx 0.03$ [1] i.e. very low wavemaking resistance;

The domain used in this study kept the size ratio used in preliminary study 2, however a scale of 1:1 was used, which means that, since the structure has a circumscribed diameter of $136.3m$, the domain is $16083.4m$ long (x), $13902.6m$ wide (y) and $6015m$ high (z). The center of the structure is located $5452m$ away from the inlet and $6951.3m$ from the lower part of the domain.

3.4. Boundary Conditions

For the first and second set of simulations, similar boundary conditions to those used by Khaledi and Andersson [6] were used:

Imposed velocity at the inlet: uniform flow with streamwise velocity vector, $\mathbf{V} = (\mathbf{1}, \mathbf{0}, \mathbf{0})[m/s]$. k and ω are specified and pressure, p, is extrapolated. An inlet turbulent intensity of $I = 1 \times 10^{-2}$ gives $k = 1.5 \times 10^{-4} U_\infty^2 [m^2/s^2]$. Using $\frac{\nu_t}{\nu} = 1 \times 10^{-4}$, ω follows from: $\omega = \frac{k}{\nu_t}[1/s]$; Mirror conditions at side walls of the domain to simulate an infinitely long cylinder, $V_z = 0$; Zero-pressure condition at the outlet of the domain and zero streamwise derivatives for the remaining quantities, $\frac{\partial\phi}{\partial x} = 0$; Free-slip conditions at the top and bottom boundaries: null normal velocity component ($V_y = 0$) and zero normal derivatives for the remaining quantities, $\frac{\partial\phi}{\partial y} =$

[1] g is the acceleration of gravity, L is the characteristic length

0; No-slip and impermeability condition at the wall of the cylinder. All velocity components equal to the wall velocity, normal pressure derivative is zero.

In the second preliminary study the use of wall functions was evaluated [5]. Two alternatives were tested to determine the shear-stress at the wall τ_w and the specification of the ω boundary condition[2]:

- No wall functions (NO): τ_w is determined directly from its definition and the near-wall analytical solution of the ω transport equation [17] is used to specify ω at the near wall centre.
- "Automatic" wall functions (WF): These blend the analytical equations available for the linear and log layers to obtain expressions valid from the upper edge of the log layer down to the wall. Equations for the blending used in this work can be found in [5, 14].

Due to the 3D nature of the third set of simulations, a new set of boundary conditions was necessary:

Imposed velocity at the inlet; Mirror conditions at the water surface (no waves), $V_y = 0$; Zero-pressure condition at the outlet of the domain and zero streamwise derivatives for the remaining quantities; Free-slip conditions at the longitudinal top and bottom of the domain and at the 'ocean floor': null normal velocity component and zero normal derivatives for the remaining quantities. No-slip and impermeability condition at the wall of the structure. "Automatic" wall functions were used as a consequence of the results obtained in the second preliminary study.

4. Solution Procedure

4.1. Software

Mesh generation for the first preliminary study and the 3D study was done using an unstructured mesh generator: NUMECA's HEXPRESS^{TM} software. For the second preliminary study multiblock structured grids were generated using the grid generators described in [4]. Unstructured Grid refinement was done according to Crepier [2].

The software used to perform the simulations was ReFRESCO (v2.5).

4.2. Numerical Model

ReFRESCO uses a PETSc (Portable Ex-tensible Toolkit for Scientific Computation) solver for the linear equations, and the mass-momentum coupling. The convective fluxes in the momentum equations were discretised using a LIMITED QUICK scheme (QUICK scheme with a flux limiter), whereas for the turbulence equation a first order upwind (FOU) scheme was used. The time integration was performed using an implicit three-time level (2nd order) scheme for all equations, except for turbulence. In this case a first order scheme was employed, for robustness purposes [10].

4.3. Spatial Discretization

4.3.1. Preliminary Study 1

Three sets of grids were generated for the domain with the circular cylinder, six sets of grids for the domain with an hexagonal cylinder and other six sets for the domain with an octagonal cylinder (three sets for corner orientation and three for face orientation).

4.3.2. Preliminary Study 2

As previously stated, for the second set of simulations sets of structured meshes were generated using the techniques described in [3, 4].

Four sets of geometrically similar grids were generated to discretize the computational domain. The grid is orthogonal to the surface in the near-wall region and the selected topology intends to cluster cells in the near-wake region and expand the cell size at the top, bottom and outlet to avoid pressure reflections. The first set of grids (GNO) is tunned to calculate τ_w from its definition which means using the NO wall boundary conditions.

The remaining 3 sets are obtained by merging cells in the near-wall region keeping the cell height of all the grids of the same set constant. Three different values of the near-wall cell size were tested for the application of WF in sets GWF1, GWF2 and GWF3. The number of cells merged in the near-wall region of the inner block are 1/4 (GWF1), 3/8 (GWF2) and 1/2 (GWF3) of the cells in the direction perpendicular to the surface of the cylinder [5].

The grid generation strategy used for the octagonal and hexadecagonal cylinders was the same, with the number of faces on the body surface and the number of cells merges in the near-wall region for the GWF sets identical to those used for the circular cylinder [5].

4.3.3. 3D Study

For the third set of simulations, three meshes were generated using HEXPRESS^{TM}. Due to the large size of the structure and the large Reynolds number, the meshes were generated without adding a viscous layer near the wall and with the use of "automatic" wall functions.

Table 1 shows the number of faces on the surface of the structure and the total number of cells in each one of the three grids.

[2] $\omega \to \infty$ at the wall.

Table 1: Number of cells N_v, number of face elements N_f and grid refinement ratio h_i/h_1 of the grids for the simulations performed with $Re = 10^8$ with 3D geometry

Grid	N_v	N_f	h_i/h_1
1	11 379 583	388 164	1.
2	3 504 780	185 390	2.094
3	988 237	86 364	4.495

4.4. Temporal Discretization

In all cases tested, the time scale was adapted inversely to the increase of number of face elements in each refinement, in order to guarantee an average Courant number, C_{avg} close to $C_{avg} \approx 1.5$.

Table 2 shows the time scale, in seconds, used for each simulation performed with the 3D geometry.

Table 2: Time scales of the simulations performed with $Re = 10^8$ with 3D geometry, in seconds

Grid	Time Scale
1	0.177
2	0.262
3	0.4

4.5. Quantities of Interest

Each one of the three studies performed had different objectives and as such the quantities that allow to draw conclusions regarding said objectives differ between the three studies.

Preliminary study 1 had as quantities of interest: The Average force coefficients (C_D and C_L) and their evolution through time (time history), obtained from the total forces in the x and y directions; Strouhal number, obtained through an FFT (*Fast Fourrier Transform*), as a means of comparison with the literature; Average Courant number to study the presence of time errors; Convergence properties of each simulation.

Preliminary study 2 aimed to understand the impact of wall functions in the simulation, so one of the main interests lies in the convergence properties of the simulation. The relevant quantities are: Average Force coefficients and their time history; Frequency content of the time histories, by means of an FFT and Strouhal number, St; The time history of the main Cartesian velocity components U_x and U_y at two points in the near wake for the three geometries considered: P_1 has coordinates $x = 1.75d, y = 0$ and P_2 is located at $x = d, y = 0.75d$ - the interpolation is performed using the value and the gradient at the nearest cell-centre; Iterative convergence properties of the simulations.

The final and main study wants to study the forces and moments acting on the structure in order to permit an accurate structural analysis in future studies. So, naturally, the interest lies with: Time history of the forces in the three directions and respective average values; Time history and average moments acting in the three directions; Frequency content analysis of the signals of the time histories.

5. Results

5.1. Preliminary Study 1

5.1.1. Time History of the Forces and Average Force Coefficients

The evolution of the force coefficients through time was plotted for each simulation. Figure 1 shows two examples of the time history plots.

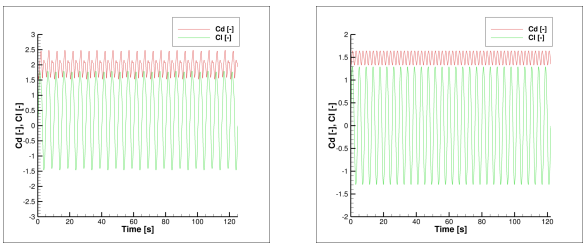

(a) Hexagonal cylinder with face orientation

(b) Circular cylinder

Figure 1: Evolution of C_d and C_L for the simulations with the most refined grid (Grid 1) using the $k - \omega SST$ model

The values of $\overline{C_d}$ and $\overline{C_l}$ are present in Tables 3 and 4, respectively, for all the simulations performed for this study, as a function of cross-section shape of the cylinder and the turbulence model used.

Table 3: Average Drag coefficient for the simulations performed with $Re = 10^3$

Grid	Turbulence Model	Circle	Hexagon		Octagon	
			Corner	Face	Corner	Face
1	$k - \omega SST$	1.4957	1.6884	1.9913	1.8727	1.5489
	$KSKL$	1.4734	1.7109	2.0354	1.8563	1.5353
2	$k - \omega SST$	1.4918	1.7224	1.9978	1.7569	1.5383
	$KSKL$	1.4648	1.7462	2.0442	1.7368	1.5229
3	$k - \omega SST$	1.5102	1.7591	2.0232	1.7049	1.6012
	$KSKL$	1.4795	1.7778	2.1945	1.8640	1.5771

From the average values of the force coefficients it is evident that there is little difference between the several refinement levels for a given case, particularly in the average Drag coefficient. Larger differ-

Table 4: Average Lift coefficient for the simulations performed with $Re = 10^3$

Grid	Turbulence Model	Circle	Hexagon		Octagon	
			Corner	Face	Corner	Face
1	$k-\omega SST$	4.1750×10^{-5}	-0.15637	0.31461	0.063454	2.6420×10^{-5}
	$KSKL$	1.8780×10^{-5}	0.11519	0.021897	1.9880×10^{-4}	2.7510×10^{-5}
2	$k-\omega SST$	1.5350×10^{-5}	0.15377	-0.30218	-0.16871	9.8530×10^{-5}
	$KSKL$	1.499×10^{-5}	0.11281	0.082789	0.0014072	1.0040×10^{-4}
3	$k-\omega SST$	1.612×10^{-5}	0.11378	-0.26432	-1.9404×10^{-4}	4.317×10^{-5}
	$KSKL$	1.664×10^{-5}	0.062869	-0.093386	2.1532×10^{-4}	3.946×10^{-5}

ences between the refinement levels on the average Lift coefficient can be due to the fact that forces in the y-direction vary more heavily through time.

5.1.2. Strouhal Number

An FFT was used to obtain the Strouhal number since it allows to analyse the frequency content of a solution.

In [6] the values obtained are $St = 0.1718$ for an hexagonal cylinder with corner orientation and $St = 0.2136$ for an hexagonal cylinder with face orientation. For the circular cylinder, reference values can be found [16] and [9], where values close to $St = 0.21$ are obtained for uniform flow around a circular cylinder at $Re = 1000$.

The values of Strouhal number obtained in this study are presented in Table 5.

Table 5: Strouhal number obtained for the simulations performed with $Re = 10^3$

Grid	Turbulence Model	Circle	Hexagon		Octagon	
			Corner	Face	Corner	Face
1	$k-\omega SST$	0.2376	0.1908	0.1997	0.2613	0.2152
	$KSKL$	0.2365	0.1977	0.2087	0.2614	0.2153
2	$k-\omega SST$	0.2361	0.1931	0.2001	0.2369	0.2158
	$KSKL$	0.2345	0.2003	0.2092	0.2409	0.2155
3	$k-\omega SST$	0.2365	0.2010	0.1996	0.2342	0.2152
	$KSKL$	0.2345	0.2080	0.2236	0.2532	0.2145

The similarity of the results here obtained with the literature available helps to confirm that the use of unstructured grids and Crepier's refinement method [2] is not a disadvantage when dealing with complex geometries.

5.1.3. Average Courant Number

High values of Courant number, C_{avg}, indicate the presence of significant time erros. Acceptable values of C_{avg} are as close to one as possible, since it shows that the time scale and the spatial scale are well adapted to each other. Table 6 shows C_{avg} obtained for each simulation.

As Table 6 shows, C_{avg} of all the simulations performed at this stage is below 1.6.

Table 6: Average Courant number C_{avg} obtained for the simulations performed with $Re = 10^3$

Grid	Turbulence Model	Circle	Hexagon		Octagon	
			Corner	Face	Corner	Face
1	$k-\omega SST$	1.28247	1.07209	1.55460	1.32202	1.16588
	$KSKL$	1.18062	1.06582	1.35405	1.41031	1.22798
2	$k-\omega SST$	1.25368	1.26615	1.50999	1.51988	1.18434
	$KSKL$	1.28533	1.21465	1.38345	1.47383	1.13029
3	$k-\omega SST$	1.36489	1.14386	1.44204	1.45579	1.28321
	$KSKL$	1.32384	1.13492	1.44945	1.46792	1.16369

5.1.4. Convergence Properties

The average number of iterations per time step for the simulations with the circular cylinder was close to 25 for Grids 2 and 3 and close to 30-35 for the simulations with Grid 1, regardless of the turbulence model. For the polygonal cases, with both orientations, Grids 2 and 3 performed at about 25 iterations per time-step and for Grid 1 it was close to 70 iterations per time-step. This shows that all the simulations converge properly. For the finest grid there is a steep increase in average number of iterations per time step, particularly in the more complex geometries, which was to be expected, given the decrease in grid size. This shows that with more complex geometries and very small grid sizes, the simulation will be significantly more computationally expensive.

5.1.5. Conclusions From This Study

It is clear that the behaviour of circular, hexagonal and octagonal cylinders in turbulent flow has relevant differences. As the number of faces increases in a polygonal cylinder, similarities with the circular cylinder start to become apparent.

Additionally, it is possible to conclude that the results obtained with unstructured grids are accurate and that using unstructured grids provides stable simulations with an acceptable convergence.

5.2. Preliminary Study 2

5.2.1. Circular Cylinder

The time histories show that, for all simulations performed, all the quantities under analysis become periodic. Grid and time refinement, as well as the selected wall boundary condition is shown to affect differently the selected quantities.

C_D has a period that is half of that determined for C_L, which was expected. The signals of two velocity components of the point located outside the boundary layer (P_2) have the same period of C_L, while, for the point in the near-wake (P_1), V_y has the same period of C_L and V_x has half of that period, behaving as C_D.

The results suggest that the solutions produced by the simulations show "RANS-like" behaviour. This is confirmed by the frequency content of the signals of the time histories of the quantities of interest.

The FFTs of all simulations exhibit sharp peaks only at discrete frequencies, however force coefficients show only one frequency, while the plots of V_x and V_y at P_1 (near-wake) exhibit more than one. Regarding the point outside of the viscous region, P_2, the plots of V_x and V_y present the same frequency as C_L but the second harmonic is also present.

There is a remarkable consistency between the results obtained without wall functions (GNO) and those obtained with wall functions for the minimum and maximum values of near-wall cell size (GWF1 and GWF3), however the same is not true for the data obtained with the set GWF2. There is a significant discrepancy between the data obtained with this grid set and the remaining simulations that cannot be explained by numerical uncertainty. This is an awkward result, given that it suggest that wall functions could be acceptable for bluff bodies at very high Reynolds numbers, but it also shows that there is a strong influence of the size of the near wall cell on the force coefficients determined with wall functions [5].

The results show that only the GNO, GWF1 and GWF3 are consistent for all four quantities of interest. The results from the GWF2 grid set present discrepancies relative to the remaining simulations. This means that the results do not change monotonically with the increase in near-wall cell height. But the grids with the largest near-wall cell size show the largest numerical uncertainties.

The results obtained for this geometry seem to indicate that at very high Reynolds numbers, wall functions significantly enhance the robustness of the simulations compared to the calculation of τ_w from the definition.

Figure 2 illustrates the streamlines and V_x field at a time instant close to minumum lift coefficient for the finest grids/smallest time-step of the four grid sets tested. There is a remarkable resemblance between the GNO, GWF1 and GWF3 graphics. The GWF2 graphic shows a larger vortex and wider near-wake, which explain the results obtained for this grid set.

5.2.2. Octagonal Cylinder

For this geometry, for the simulations performed without wall functions, iterative convergence was extremely difficult to achieve. The ratio between the maximum and average Courant number is significantly larger than what was obtained for the circular cylinder.

The time histories of the lift and drag coefficients obtained with the coarsest grid of sets GNO and GWF show a "RANS-like" behaviour. The statistical convergence appears to be better for the grid set with wall functions (GWF1) compared to the one without wall functions (GNO). On the other hand, grid/time refinement leads to an increase of the iterative convergence problems at each time step for the GWF1 set, so only the other two wall function sets (GWF2 and GWF3) will be further analysed.

From the time histories of the lift and drag coefficients obtained in the GWF2 set [3] it is possible to see that the coarsest grids are the only ones that exhibit a periodic behaviour with discrete frequencies in the force coefficient time histories. Grid/time refinement lead to an increase in the range of frequencies present in the time histories under study. This suggests that the turbulence model (as well as numerical diffusion) are not enough to obtain a RANS solution. This makes it difficult to assess statistical convergence or even to define a cycle.

The values obtained for the force coefficients with this geometry are significantly larger than the ones obtained for the flow around the circular cylinder. More, the Strouhal number is close to half of that obtained for the circular cylinder, which seems to indicate that the wake is wider for the octagonal geometry.

It is also evident that the increase in size of the "viscous region" is due to the kinks on the surface of the cylinder that provoke flow separation. Although the time histories suggest that this solution does not correspond to the "RANS-like" solution that was expected, the width of the wake is similar in the two simulations, unlike what was obtained with the circular cylinder for these two grid sets.

5.2.3. Hexadecagonal Cylinder

The Courant number was maintained close to 0.3 for all grid sets to achieve iterative convergence in a reasonable number of iterations per time-step. Regardless, simulations with the coarsest grid of the

[3] The simulation of the finest grid of this set was not performed.

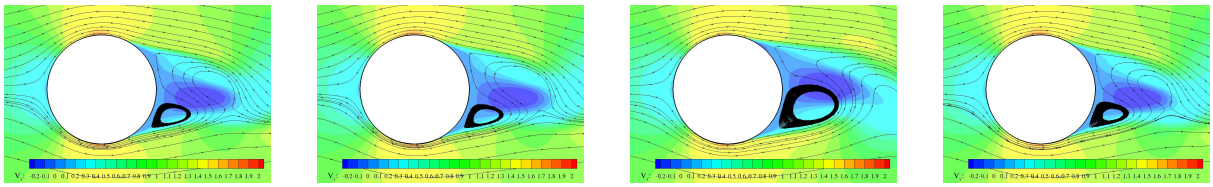

(a) GNO (b) GWF1 (c) GWF2 (d) GWF3

Figure 2: Visualization of the flow field and isolines of V_x at a time close to minimum lift coefficient $(C_L)_{min}$ obtained in the finest grids with the smallest time step. Flow around a circular cylinder at a Reynolds number of 10^8 calculated with and without wall functions.

GWF1 set required approximately 2000 iterations to reduce the L_∞ norm of the normalized residuals to 10^{-4}, so the simulations for this set were not completed. For the coarsest grid of the GNO set, about 500 iterations were required to lower the residuals to 5×10^{-5}.

The time history results suggest that more simulation time is required to achieve statistical convergence, Nevertheless, the results obtained for the force coefficients are much closer to the octagonal cylinder than the circular one.

Grid sets GWF2 and GWF3 show significantly better iterative convergence, with an average of 30 iterations per time-step with a convergence criteria of 10^{-5}. All the solutions present a "RANS-like" behaviour, but the frequency content of the force coefficients differs between the two sets.

In GWF2 the two coarsest grids show a periodic behaviour of C_L and C_D, with the lift coefficient presenting only one frequency. However, with grid/time refinement this behaviour is lost and for the finest grid several other frequencies appear in the time history of the force coefficients.

The results of GWF3 present a consistent behaviour of the time signals of the lift and drag coefficients for all the grids/time-steps tested. Statistical convergence resembles that which was obtained in the circular cylinder, thus in this case numerical uncertainty is dominated by the discretization error.

The most striking feature observed regarding the convergence with grid/time refinement of $C_{D_{avg}}$, $C_{D_{max}}$, $C_{L_{rms}}$ and St for the simulations performed using GWF2 and GWF3 is that none of the quantities of interest present monotonic convergence. The largest uncertainties are, once again, obtained for the GWF3 set.

The force coefficients obtained for this cylinder are closer to the ones from the octagonal cylinder than those from the circular cylinder. However, there is a reduction of the average drag coefficient which suggests a reduction, however small, of the width of the wake in comparison to the octagonal cylinder.

5.2.4. Conclusions From This Study

It is possible to conclude that the use of wall functions significantly improves the robustness of the flow solver; The only noticeable systematic trend in the three test cases seems to be that there is a significantly increase in numerical uncertainty of the quantities under investigation for the largest near-wall cell size;

The results from the simulations of flow around the octagonal cylinder did not present a "RANS-like" behaviour, which was present in the flow around the circular cylinder for all grid/time steps tested. For the hexadecagonal cylinder "RANS-like" solutions were obtained but the frequency content is strongly dependent on the refinement level for one of the grid sets. Thus it is impossible to know whether or not the turbulence model is capable of providing the necessary diffusion to damp the turbulent fluctuations.

The results show that even at such high Reynolds numbers it is the kinks on the surface of the polygonal cylinders that produce a significant increase of the force coefficients.

This seems to suggest that wall functions can be an efficient option to simulate very high Reynolds numbers flows around bluff bodies, but also that the size of the near-wall cells have a strong influence on the solution. [5].

5.3. 3D Study

For the 3D case it is relevant to study the average values of forces and moments at which the structure will be subject to, as well as the frequency content of the simulation. The moments are being calculated with respect to the point $(x, y, z) = (5452, 6951.3, 6815)[m]$.

5.3.1. Time History of the Forces and Moments

In the previous studies, the initial part of the simulation, under the effect of the initial condition was discarded and the most relevant part of the information was extracted to be analysed. However, in the simulations performed in this part of the investigation, the results obtained do not show a periodic behaviour, which means that, while average

values can be extracted and a frequency analysis performed, it is hard to judge the statistical convergence of the simulations.

Both the forces and moments acting on the structure show a non- "RANS-like" behaviour similar to what was obtained in the second preliminary study.

The frequency analysis shows that it is not possible to identify one dominant frequency. Therefore it is not possible to extract a Strouhal number. This type of frequency behaviour seems to be closer to what was to be expected from a fully turbulent regime as opposed to a RANS simulation. It is even possible to find a frequency region where the log-log plot seems to have a linear slope, which would be consistent with Kolmogorov's $-5/3$ rule [7, 8].

This behaviour suggests that the diffusion offered by the turbulence model was not able to dampen some of the turbulent frequencies at such a high Reynolds number, as was the case of the octagonal cylinder analysed in the second preliminary study.

Nonetheless some information can still be taken from these results, namely regarding the average values of the forces and moments, which can be seen in Table 7.

It is evident that the force in the y-direction (F_y) is several orders of magnitude smaller than the forces in the streamwise direction of the flow F_x and, more notably, than the force in the vertical direction F_z. The reason for the latter is most likely related to the tapered geometry of the net, which creates a zone of high flow velocity and therefore low pressure in the bottom of the net, due to the formation of large vortexes in the bottom of the structure, pushing the structure downwards. It is reasonable to assume that similar simulations where the net is computed as a permeable, deformable surface will result in a lower absolute values of F_z and F_x, since the net will no longer display the same behaviour as it does in this study.

Table shows that the moments in the vertical direction are smaller than the ones in the other directions, which was to be expected given the symmetry of the structure.

Regarding the average moments in y-direction, which are several orders of magnitude larger than the moments in the other two directions, this is consistent with the fact that the forces in the streamwise direction, F_x, and the force in the vertical direction, F_z, have the most magnitude of the forces acting on the structure, since this is the pair of forces that will generate M_y. Again, the magnitude of this moment is expected to be smaller in a simulation where the net is deformable and permeable.

From Figures 3 (a) and (b) it is possible to see that, away from the structure, in the hanging nodes from the largest cell size to the second largest cell size there exists some numerical error affecting the flow, however, since this behaviour is far away from the structure (more than $30d$ away from the structure, the influence of this numerical artifact on the results obtained should be minimal.

Figure 3 (c) shows that the wake created by the structure is more than $17d$ long and Figure 3 (d) show the increase in flow velocity under the structure due to the tapered geometry of the structure and the angle formed by the sides and the bottom of the net, which leads to the formation of a vortex underneath the structure in addition to the ones formed in the wake of the bluff body.

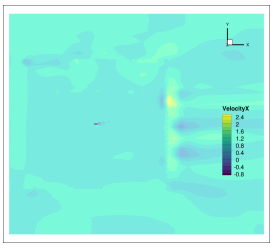

(a) Top-down View ($x-y$ plane)

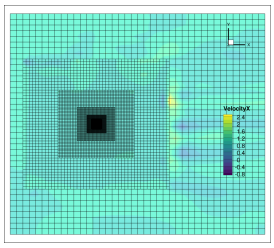

(b) Top-down View ($x-y$ plane): Overlayed grid

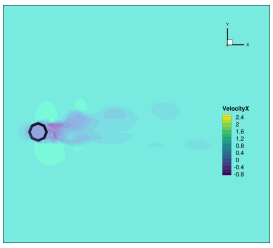

(c) Top-down View ($x-y$ plane): Close-up of the structure

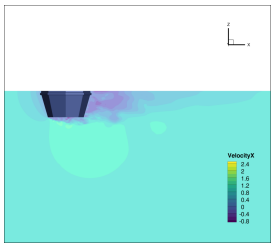

(d) Side View ($x-z$ plane): Close-up of the structure

Figure 3: Instantaneous velocity plots, at the last time-step using Grid 1.

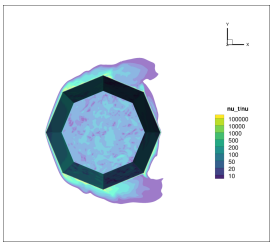

(a) Top-down View ($x-y$ plane): Close-up of the structure

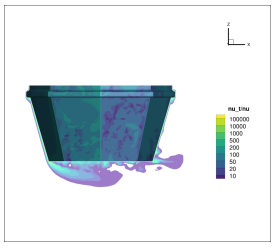

(b) Side View ($x-z$ plane): Close-up of the structure

Figure 4: ν_t/ν plots, at the last time-step - Grid 1.

In Figure 4 all regions of the flow with $\nu_t < 2\nu$ are left white, so that the only the "viscous region" of the flow is visible. It is evident that the influence of turbulence in the flow is very low, since only the region close to the wall and the near wake have val-

Table 7: Average value of forces and moments for the simulations performed with a 3D Aquaculture Structure, $Re = 10^8$

	$\overline{F_x}$ $[N]$	$\overline{F_y}$ $[N]$	$\overline{F_z}$ $[N]$	$\overline{M_x}$ $[N/m]$	$\overline{M_y}$ $[N/m]$	$\overline{M_z}$ $[N/m]$
Grid 1	2279.998	-173.5992	-2014.156	-3186.399	-39375.01	1556.972
Grid 2	2432.406	-32.81141	-1637.040	-707.7282	-45584.81	-41.25015
Grid 3	2254.789	-182.3948	-1206.320	-2706.553	-41505.71	1451.078

ues of eddy viscosity over 2ν. This explains the frequency behaviour seen previously, since there does not seem to be enough diffusion from the turbulence model to dampen the turbulent fluctuations at the Reynolds number of the simulation.

5.3.2. Conclusions From This Study

This study allows to make some estimations regarding the average value of the forces acting on the structure: the force in the x-direction is in the vicinity of 2300 N, the force in the y-direction should be a little under 200 N, while the force in the z-direction is near 2000 N. An estimation of the average value of the moments is also possible, with the moments around x close to -3000 N/m, the moments around y are clearly the strongest moments acting on the structure, about 40000 N/m and the moments in the z-direction approximately 1500 N/m.

Not much can be said about the frequency behaviour since the results obtained did not show a "RANS-like" behaviour, but given that the available literature on flow around bluff bodies at such a high Reynolds number is not extensive enough, comparisons are not possible.

The size of the near-wall cells is most likely too large which contributed to values of eddy viscosity which are too low. It was not possible to generate a new grid and perform new simulations due to time and computational constraints.

From a computational point of view, given the size of the domain and complexity of the structure it is clear that the choices regarding the use of unstructured grids and the use of wall functions, made with the knowledge taken from the two preliminary studies, were appropriate choices, since the computational time used allowed for the extraction of useful information from the simulations without rendering the simulations prohibitively expensive. Even so, with as much computational resources as were used in this case, the results obtained are still not ideal. A lot more investigation can be made in this field, both in terms of the use of unstructured grids, perhaps with smaller grid sizes or with smaller cell size jumps in the far field, and in terms of the use of wall functions at this Reynolds numbers. These investigations, motivated by projects such as off-shore aquaculture structures or off-shore wind turbine installations, will be able to better predict the behaviour of bluff bodies in very high Reynolds number flows.

6. Conclusions

The first preliminary study made clear the differences in the behaviour of the flow around cylinders with three different cross section geometries. It also showed that the simulations performed with unstructured grids showed the necessary robustness, allowing for stable simulations with acceptable convergence.

The second preliminary study showed that the use of wall functions improved the robustness of the simulations. A significant increase in numerical uncertainty for the largest near-wall cell size for all grid sets was reported. The circular cylinder was the only where "RANS-like" solutions resulted from all the simulations. Consequently it is not possible to understand if this is caused by lack of diffusion from the turbulence model. This study suggested that wall functions can be an efficient option to simulate very high Reynolds numbers flows around bluff bodies, but that the size of the near-wall cells have a strong influence on the solution.

Concerning the final 3D study, estimations were made regarding the average values of forces and moments acting on the surface of the structure. The frequency content did not show a "RANS-like" behaviour. The near wall cell size used in the 3D study was most likely too large and as such the levels of eddy-viscosity are too low. Generation of a new grid was not possible. Given the complexity of the structure and computational time expended on the simulations there is confidence in the computational choices made in the final study.

Further investigations of flows at very high Reynolds numbers are recommended, given that this is a quasi-unexplored area of fluid dynamics.

The use of wall functions seems to be acceptable at very high Reynolds numbers but the high influence of the size of the near-wall cell on the force

coefficients needs to be analysed by means of a sensitivity study for the near-wall cell size.

Acknowledgements
The author would like to thank Professor Luís Eça for the opportunity to work in this project within the collaboration IST/MARIN. The author would also like to thank NUMECA for allowing use of their mesh generator, HEXPRESS.

References

[1] R. M. Costa and L. Eça. Assessing rans numerical and modelling properties in the simulation of the flow around fixed and moving cylinders. Master's thesis, Universidade de Lisboa - Instituto Superior Técnico, 2019.

[2] P. Crepier. Ship resistance prediction: Verification and validation exercise on unstructured grids. In *MARINE 2017 Computational Methods in Marine Engineering VII*. International Center for Numerical Methods in Engineering (CIMNE), 2017. ISBN: 978-84-946909-8-3.

[3] L. Eça. Grid generation tools for structured grids. Technical report, MARIN/IST Cooperative Research Project, May 2003.

[4] L. Eça, M. Hoekstra, and J. Windt. Practical Grid Generation Tools with Applications to Ship Hydrodynamics. In *8th international Conference on Numerical Grid Generation in Computational Field Simulations*, Honolulu, Hawaii, U.S.A., June 2002.

[5] L. Eça and G. F. Neves. On the Simulation of Very High Reynolds Number Flows Around Bluff Bodies Using the RANS Equations. Technical report, Instituto Superior Técnico/MARIN Partnership, 2020.

[6] H. A. Khaledi and H. I. Anderson. On vortex shedding from a hexagonal cylinder. *Physics Letters A*, 2011.

[7] A. N. Kolmogorov. Dissipation of Energy in the Locally Isotropic Turbulence. In *Proceedings of the Royal Society A: Mathematical, Physical and Engineering Sciences*, August 1991.

[8] A. N. Kolmogorov. The Local Structure of Turbulence in Incompressible Viscous Fluid for Very Large Reynolds Numbers. In *Proceedings of the Royal Society A: Mathematical, Physical and Engineering Sciences*, August 1991.

[9] M. Kyia, H. Tamura, and M. Arie. Vortex shedding from a circular cylinder in moderate-Reynolds number shear flow. *Journal of Fluid Mechanics*, 141, 1980.

[10] MARIN. ReFRESCO Controls Documentation, version 2.5.0.

[11] F. Menter. Two-equation eddy-viscosity turbulence models for engineering applications. *AIAA Journal*, 32(8), 1994.

[12] F. Menter and Y. Egorov. The scale-adaptive simulation method for unsteady turbulent flow predictions. part 1: Theory and model description. *Flow, Turbulence and Combustion*, 85:113–138, 2010.

[13] F. Menter, Y. Egorov, and D. Rusch. Steady and Unsteady Flow Modelling Using the $k\sqrt{kl}$ Model. In *Proceedings of the International Symposium on Turbulence, Heat and Mass Transfer, vol 5, p.403-406*. Ichmt Digital Library Online. Begel House Inc., 2006.

[14] F. Menter and T. Esch. Elements of industrial heat transfer predictions. In *16th Brasilian Congress of Mechanical Engineering*, 2001.

[15] F. Menter, M. Kuntz, and R. Langtry. Ten Years of Industrial Experience with the SST Turbulence Model. *Turbulence, Heat and Mass Transfer*, 4, 2003.

[16] C. Norberg. An experimental investigation of the flow around a circular cylinder: influence of aspect ratio. *Journal of Fluid Mechanics*, 258, 1994.

[17] D. Wilcox. *Turbulence Modeling for CFD*. DCW Industries, 2006.

[18] S. J. Xu, W. Zhang, L. Gan, and Y. Zhou. Experimental study of flow around polygonal cylinders. *Journal of Fluid Mechanics*, 812:251–278, 2017.